Mathematical Biosciences and Engineering

MBE, 19(12): 13214–13226.
DOI: 10.3934/mbe.2022618
Received: 20 July 2022
Revised: 02 September 2022
Accepted: 05 September 2022
Published: 09 September 2022

http://www.aimspress.com/journal/MBE

Research article

Sparse reconstruction of magnetic resonance image combined with two-step iteration and adaptive shrinkage factor

Xiuhan Li[1,†], Rui Feng[1,†], Funan Xiao[2,†], Yue Yin[3], Da Cao[4], Xiaoling Wu[1], Songsheng Zhu[1,*] and Wei Wang[1,*]

[1] Key Laboratory of Clinical Engineering, School of Biomedical Engineering and Informatics, Nanjing Medical University, Nanjing 211166, China
[2] Jiangsu Province Hospital of Chinese Medicine, Affiliated Hospital of Nanjing University of Chinese Medicine, Nanjing 210029, China
[3] Department of Medical Engineering, Jiangbei Branch of Zhongda Hospital Affiliated to Southeast University, Nanjing 210044, China
[4] Department of Radiology, The First Affiliated Hospital of Nanjing Medical University, Nanjing, 210029, China

† The authors contributed equally to this work.

* **Correspondence:** Email: zhu@njmu.edu.cn, bmeww@njmu.edu.cn; Tel: +8602586869350.

Abstract: As an advanced technique, compressed sensing has been used for rapid magnetic resonance imaging in recent years, Two-step Iterative Shrinkage Thresholding Algorithm (TwIST) is a popular algorithm based on Iterative Thresholding Shrinkage Algorithm (ISTA) for fast MR image reconstruction. However TwIST algorithms cannot dynamically adjust shrinkage factor according to the degree of convergence. So it is difficult to balance speed and efficiency. In this paper, we proposed an algorithm which can dynamically adjust the shrinkage factor to rebalance the fidelity item and regular item during TwIST iterative process. The shrinkage factor adjusting is judged by the previous reconstructed results throughout the iteration cycle. It can greatly accelerate the iterative convergence while ensuring convergence accuracy. We used MR images with 2 body parts and different sampling rates to simulate, the results proved that the proposed algorithm have a faster convergence rate and better reconstruction performance. We also used 60 MR images of different body parts for further simulation, and the results proved the universal superiority of the proposed algorithm.

Keywords: compressed sensing; MR imaging reconstruction; iterative shrinkage thresholding; two-step iterative; dynamic shrinkage factor

1. Introduction

Nyquist sampling theorem is the criterion that must be followed in traditional image acquisition system. The traditional acquisition mode often acquires raw image data at a very high sampling frequency, it may take a long time and require high equipment performance. The same, traditional magnetic resonance (MR) imaging also takes too long time, which is easy to cause motion artifacts, and patient compliance is poor. In addition, for imaging that requires injection of contrast agents, prolonged sampling can result in reduced contrast, which can result in poor quality or undiagnosable images.

In order to solve the above problems, Compressed Sensing (CS) theory was proposed [1], based on the theory of sparse decomposition and signal approximation. In this theory, the raw data which are undersampled can be reconstructed by performing nonlinear optimisation, and without reducing the image quality. In 2007, CS was applied to the field of MR imaging and achieved amazing results [2]. After that, efficient reconstruction algorithms had always been a research hotspot in undersampling MR image reconstruction field. Among them, Iterative shrinkage thresholding algorithm (ISTA) [3], Split Bregman Iteration [4] and conjugate gradient (CG) [5] were the mostly used algorithms. Compared with Bregman and CG, ISTA had lower algorithm complexity and directly solved the L1 minimization problem to get faster iterations [3, 6–9]. In addition, with the deepening of deep learning in medical image processing research, it also provides new solutions for fast magnetic resonance reconstruction [10,11].

Therefore, a large number of people have studied the ISTA algorithm to improve the reconstruction accuracy and improve the iterative efficiency, and a series of improved ISTA were brought up. In 2007, Bioucas-Dias and Figueiredo [12] proposed Two-step Iterative Shrinkage Thresholding Algorithm (TwIST), the first two iteration estimates and threshold functions are used to estimate the current value at each iteration. In 2009, Beck et al. [13] proposed Iterative shrinkage thresholding algorithm (FISTA) based on the results of the first two iteration to improve global rate of convergence. In 2015, Zhang et al. [14] proposed an algorithm used exponential wavelet as sparse transformation, it can improve MR image reconstruction effect by increasing signal sparsity. In 2015, Li et al. [15] proposed Hessian Schatten norm-based regularization instead of the total variation (TV), it can keep the favorable properties of TV and reduce the staircase effect appearing in TV-based reconstructions. In 2016, Wu et al. [16] used regularization parameter to be taken as a threshold in a fixed-point ISTA. In 2019, Shang et al. [17] proposed an easy-to-implement algorithm based on the framework of alternative direction method, named iterative p-shrinkage thresholding algorithm (PISTA), for solving the low Tucker rank tensor recovery problem. And it has been successfully applied in MRI image recovery.

However, in order to improve the efficiency of the iteration, early in the iterations, the weight of the fidelity term should be increased to speed up the convergence. Late in the iterations, the weight of the regular term should be increased to improve the convergence accuracy. But in above algorithms, the weight of fidelity item and regular item are fixed. In this paper, two-step iterative Thresholding Algorithm with dynamic shrinkage factor (DTwIST) was proposed, DTwIST can dynamic adjust

shrinkage factor to rebalance the weight of fidelity item and regular item to improve the convergence efficiency, and can improve the final convergence accuracy.

2. Materials and methods

2.1. Magnetic resonance imaging model under compressed sensing

To apply the theory of compressed sensing to rapid imaging of magnetic resonance, the first is to use part of k-space data obtained by undersampling as a known condition, and then use the a priori knowledge of the sparseness of the magnetic resonance image in the specific transform domain, and then construct the convex optimization problem of L1 norm in combination with the compressed sensing theory, at last an optimal solution for the magnetic resonance image can be got. The basic mathematical model is shown as follows:

$$\arg\min \| \Psi u \|_1 \quad s.t. \| F_u u - y \|_2^2 < \varepsilon \tag{1}$$

where u is the magnetic resonance image to be reconstructed, Ψ stands for linear sparse transform, it can be total variation (TV), wavelet transform, curvelet transform or other sparse transform, F_u stands for k-space sampling mode, y is the k-space data obtained by undersampling measurement, ε represents the noise level of the measured data. Because k-space data is a two-dimensional Fourier transform of magnetic resonance images, the measurement matrix in the model is the undersampled Fourier transform matrix. Convert Eq (1) into unconstrained optimization problem form by lagrange multiplier method:

$$\arg\min \| F_u u - y \|_2^2 + \alpha \| \Psi u \|_1 \tag{2}$$

The regularization parameter α in Eq (2) is used to balance the proportion of the fidelity term $\| F_u u - y \|_2^2$ with the regular term $\| \Psi u \|_1$. The sparse transform domain coefficient of MR image u is m, which defines as follows:

$$m = \Psi u \tag{3}$$

Ψ is an orthogonal matrix, and thus its transpose is equal to its inverse, Eq (2) can be rewritten as follows:

$$\arg\min \| F_u \Psi^T m - y \|_2^2 + \alpha \| m \|_1 \tag{4}$$

Reconstructed magnetic resonance images can be obtained by solving Eq (4).

2.2. Reweighted iterative shrinkage thresholding algorithm

RISTA mainly uses the first two reconstructed results to adjust the weights α of the fidelity and

regular item. The specific process of RISTA for solving Eq (2) is as blow.

Let $f(m) = \| F_u \Psi^T m - y \|_2^2$ and $g(m) = \| m \|_1$

Therefore solving Eq (4) is equivalent to solving the following Eq:

$$\arg\min f(m) + \alpha g(m) \tag{5}$$

Suppose $f(m)$ satisfies the condition of being Lipschitz continuous. Then, it can be approximated as follows near previous iteration m_{k-1}.

$$f(m) = f(m_{k-1}) + \left\langle m - m_{k-1}, \nabla f(m_{k-1}) \right\rangle + \frac{L}{2} \left\| m - m_{k-1} \right\|_2^2 \tag{6}$$

where L is the lower bound of the derivative of $f(m)$, called Lipschitz constant, and k is the current number of iterations. Combining the gradient descent method, a more general quadratic approximation model is used to solve the optimization problem of Eq (5).

$$m_k = \arg\min \left\{ f(m_{k-1}) + \left\langle m - m_{k-1}, \nabla f(m_{k-1}) \right\rangle + \frac{L}{2} \left\| m - m_{k-1} \right\|_2^2 + \alpha g(m) \right\} \tag{7}$$

After ignoring the constant term m_{k-1} and $\nabla f(m_{k-1})$, the above Eq (7) can be changed into the following:

$$m_k = \arg\min \left\{ \frac{L}{2} \left\| m - (m_{k-1} - \frac{1}{L} \nabla f(m_{k-1})) \right\|_2^2 + \alpha g(m) \right\} \tag{8}$$

Based on separable characteristics of L1 norm and the square of the L2 norm, Eq (8) can be solved as following 3:

$$m_k = G_k (m_{k-1} + C^T y - C^T C m_{k-1}) \tag{9}$$

where $C = F_u \Psi^T$, the function $G_k(x)$ is defined as Eq (10):

$$G_k(x) = \operatorname{sgn}(x) \max(|x| - \alpha, 0) \tag{10}$$

where $\operatorname{sgn}(x)$ is a symbolic function, α is a constant and determines the basic shrinkage step size for each iteration thresholding.

2.3. Two-step iterative thresholding algorithm with dynamic shrinkage factor

Here we introduced a dynamic shrinkage factor μ_k in Eq (10) to dynamically adjust α. Then Eq (10) can be rewritten as:

$$G_k(x) = \mathrm{sgn}(x)\max(|x| - \mu_k\alpha, 0) \tag{11}$$

The update function of the regularization parameter μ_k is updated as follows:

$$\mu_k = \mu_{k-1}\left(\frac{\left\|m_{k-1} - m_{k-2}\right\|_2}{\left\|m_{k-1}\right\|_2}\right)^{\sigma} \tag{12}$$

where m_{k-1} and m_{k-2} are the results of the previous two iterations. As the number of iterations increases, $\| m_{k-1} - m_{k-2} \|_2$ tends to zero and μ_k tends to 1. By way of adjusting the regularization parameters α, the weight of fidelity items is larger in the early stage of iterations, and it is conducive to rapid convergence. But in the late iterations, the weight of regular items is larger, so that it can ensure the image reconstruction accuracy. Parameter σ is used to adjust the change rate of the regularization parameter.

Then combined with method of iterative reweighted shrinkage [13], we used the first two iteration values to adjust the current iteration value:

$$\begin{aligned} n_k &= (1-\gamma)m_{k-2} + (\gamma-\beta)m_{k-1} + \beta\, m_k \\ m_k &= n_k \end{aligned} \tag{13}$$

where m_{k-2}, m_{k-1} and m_k are the iterative values of last three times, we use Eq (13) to adjust the current iteration value. Where γ and β are calculated as follows:

$$\rho = \frac{1-\lambda_1/\lambda_2}{1+\lambda_1/\lambda_2}, \quad \gamma = \frac{2}{1+\sqrt{1-\rho^2}}, \quad \beta = \frac{2\gamma}{\lambda_1+\lambda_2} \tag{14}$$

where λ_1 and λ_2 are chosen as reference [10], here we set them as λ_1=0.001, λ_2= 1.

Next the iterative step size of the algorithm needs to be considered. In paper [18–20], the convergence of ISTA algorithm was proved and the initial value α could be chosen as below 21:

$$\alpha = \max(C^T y) \tag{15}$$

The termination condition of the image iteration is given by the following:

$$\varepsilon = abs(1 - \frac{\|m_{k-1}\|_2}{\|m_k\|_2}) \tag{16}$$

where ε is the maximum allowable error set in advance.

2.4. Algorithm implementation

The sparse transform maps the original image into the sparse domain, making the non-zero coefficients of the sparse domain more sparse. Generally different sparse transforms are available for different types of images. The requirement of the construction of the sparse transform is to make the transform coefficients of the image on the set of bases more sparse by finding a set of orthogonal bases. In the ISTA series of algorithms, two-dimensional discrete wavelet transform (DWT2) were widely used, this sparse transform was also used in this paper.

In CS-MRI, since the sparse transform is fixed, the incoherent undersampling can only be achieved by designing the measurement matrix to ensure that the RIP condition is satisfied [22,23]. In two-dimensional magnetic resonance imaging, the measurement matrix is embodied in the acquisition mode of the K space. The variable density spiral trajectories 24 was used in this experiment.

The specific algorithm implementation steps are as follows:

Algorithm 1. ***Two-step iterative Thresholding Algorithm with dynamic shrinkage factor***

Inputs:

y : undersampled observation value in k-space

ψ : discrete wavelet transform

Initialization:

$k = 1, \mu_1 = 0.9, \sigma = 1, \varepsilon = 10^{-5}, \lambda_1 = 0.001, \lambda_2 = 1$

$\alpha = \max(C^T y)$

Repeat

Update μ_k by Eq (12)

Update $G_k(x)$ by Eq (11)

Update m_k by Eq (9)

Update γ, β by Eq (14)

Renew m_k by Eq (13)

$k = k + 1;$

Until $\varepsilon < tol$

Output: reconstructed MR image $u_k = \Psi^T m_k$

3. Simulation setting

As shown in Figure 1, MR images of the abdomen and lumbar spine were selected as experimental images to test the reconstruction performance of CS-MR images. The MRI raw data came from the Department of Radiology, Jiangsu Provincial People's Hospital, and they were acquired on a 1.5T Philips Achieva scanner with a 8-channel receiver coil.

The abdomen image matrix size = 448 × 448 and the lumbar spine image matrix size = 528 × 528. To control the effect of different matrix sizes, the images are resampled before algorithm processing, and the matrix size after the two images are resampled = 512 × 512.

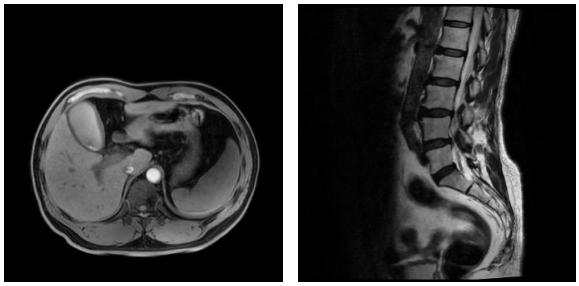

Figure 1. the full sampling images–left: abdomen, right: lumbar spine.

The sampling pattern of variable density spiral trajectories were set to 20, 30 and 40%, and they represented 5×, 3.3× and 2.5× accelerations. Spiral is a circular spiral, radial curve. It starts from the center and does not collect corner data. The spatial resolution of the image is isotropic 20% spiral sampling trajectory are shown in Figure 2.

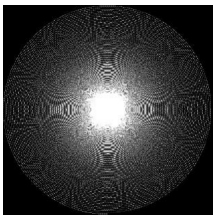

Figure 2. 20% spiral sampling trajectory.

Two general stopping criterias were used: maximum number of iterations (50) and tolerance (10^{-5}), and when either criterion is satisfied, the reconstruction stops.

ISTA, PISTA and TwIST were chosen as comparison algorithms for proposed method. The reconstruction effects were compared. 4 evaluation indicators were selected: the Peak Signal-to-Noise Ratio (PSNR in dB), Structural Similarity Index (SSIM) 25, Transferred Edge Information (TEI) 26 and normalized mutual information (NMI).

$$TEI = Q_g^{\tilde{x}\hat{x}} Q_\alpha^{\tilde{x}\hat{x}} \tag{17}$$

here, $Q_g^{\tilde{x}\hat{x}}$ and $Q_\alpha^{\tilde{x}\hat{x}}$ represent the edge strength and direction preservation values respectively. The larger the value of TEI is, the better the edge information of the reconstructed image is kept.

$$NMI(A,B) = \frac{H(A) + H(B)}{H(A,B)} \tag{18}$$

where $H(A)$ and $H(B)$ are the entropies of images A and B, respectively, and $H(A,B)$ is the joint entropy of images A and B. The larger the NMI value, the higher the similarity between the two images.

4. Results

In order to fully evaluate the performance of the proposed algorithm (DTwIST) in this paper, we have designed several sets of experiments, and ISTA, PISTA, TwIST were used as comparison algorithms.MATLAB (R2016a) is used to implement the algorithm.

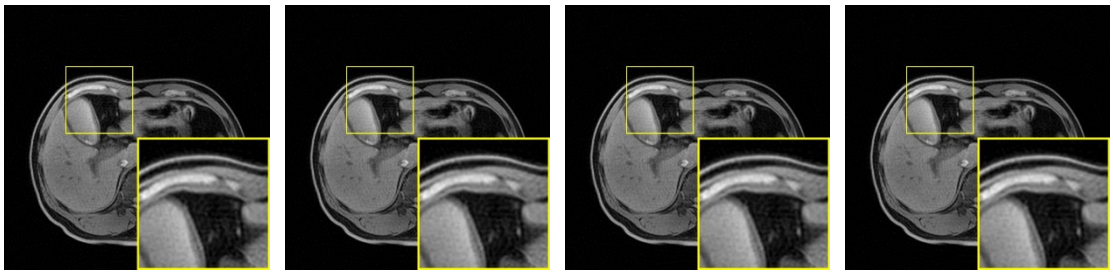

PSNR: 40.64 PSNR: 40.94 PSNR: 40.78 PSNR: 41.15

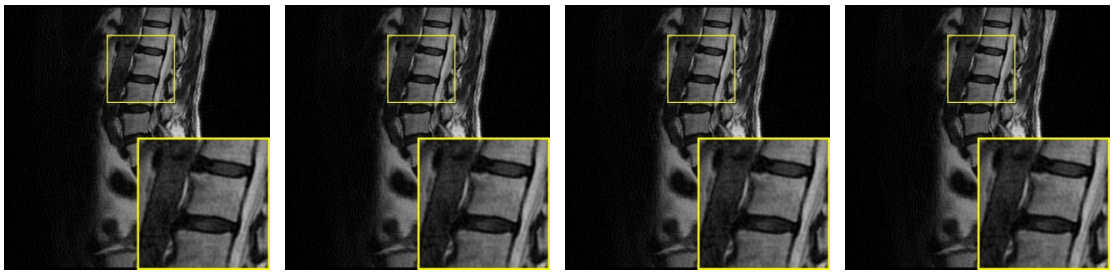

PSNR: 38.64 PSNR: 38.87 PSNR: 38.78 PSNR: 39.03

(a) ISTA (b) PISTA (c) TwIST (d) DTwIST

Figure 3. The reconstructed images and detailed images for abdomen and lumbar spine at 20% sampling rate after 50 iterations.

First, we compare the reconstruction performances of different images at the same sampling rate (20%) by 4 algorithms. Figure 3 shows the images were reconstructed by 4 different algorithms at 20% sampling rate after 50 iterations. 4 columns of images represent ISTA, PISTA, TwIST and DTwIST. The results show that the reconstructed images with DTwIST can get sharper edges and better local detail than other 3 at 20% sampling rate.

Figures 4 and 5 show the convergence curves of the reconstruction performance. PSNR, SSIM, TEI and NMI were used to quantitatively evaluate the performance of the 4 algorithms. The abscissa is the number of iteration. The results show that the image reconstructed based on DTwIST have a faster convergence rate and better reconstruction performance than the other three algorithms during the iterative process.

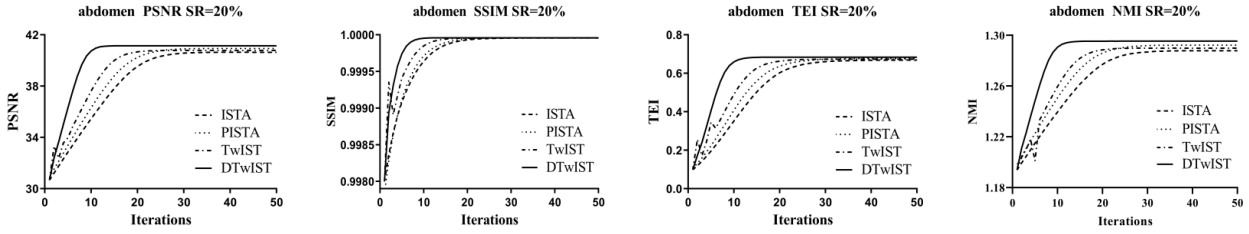

Figure 4. Performance comparisons by different evaluation indicators of abdomen MR images at 20% sampling rate.

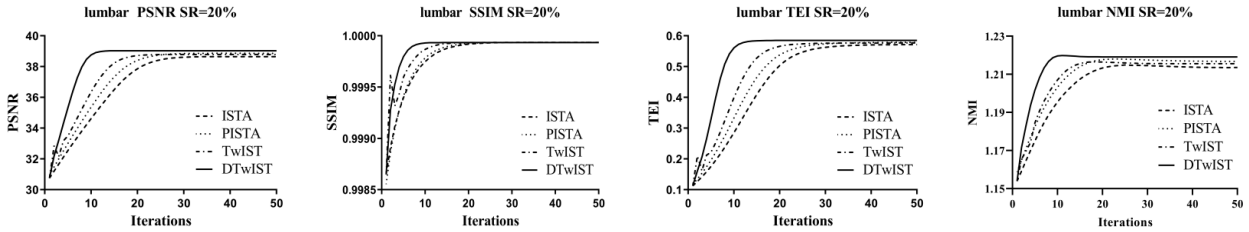

Figure 5. Performance comparisons by different evaluation indicators of lumbar spine MR images at 20% sampling rate.

Table 1 shows the numerical comparison of evaluation parameters- iterations, PSNR, SSIM, TEI and NMI reconstructed by the ISTA, PISTA, TwIST and DTwIST algorithms when the convergence iteration is stopped. The results show the superiority of DTwIST, especially excellent convergence speed.

In order to verify the applicability of the algorithm at other sampling rates. We also did experiments at 30 and 40% sampling rate.

Figures 6 and 7 show the reconstruction performance at different sampling rates after 50 iterations. PSNR, SSIM, TEI and NMI were used to quantitatively evaluate the performance of the 4 algorithms. The abscissa represents the sampling rate. The results show that the proposed algorithm has similar performance at different sampling rates.

Table 1. Performance comparison of ISTA, PISTA, TwIST and DTwIST algorithms at 20% sampling rate when the convergence iteration is stopped.

Image	Algorithms	Iterations	PSNR	SSIM	TEI	NMI
Abdomen	ISTA	36	40.64	0.9999567	0.6664	1.2876
	PISTA	38	40.94	0.9999577	0.6767	1.2922
	TwIST	25	40.78	0.9999571	0.6718	1.2897
	DTwIST	14	41.14	0.9999594	0.6820	1.2950
Lumbar spine	ISTA	37	38.65	0.9999357	0.5693	1.2140
	PISTA	38	38.87	0.9999353	0.5779	1.2170
	TwIST	26	38.79	0.9999352	0.5747	1.2159
	DTwIST	15	39.03	0.9999339	0.5840	1.2193

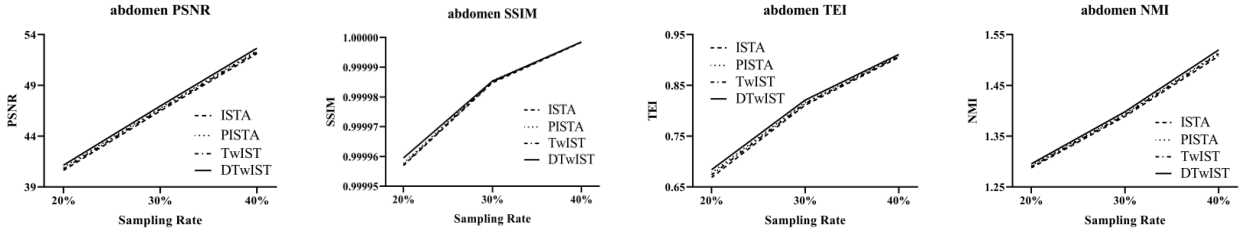

Figure 6. Performance comparison of the different algorithms for abdomen MR images under different sampling rates.

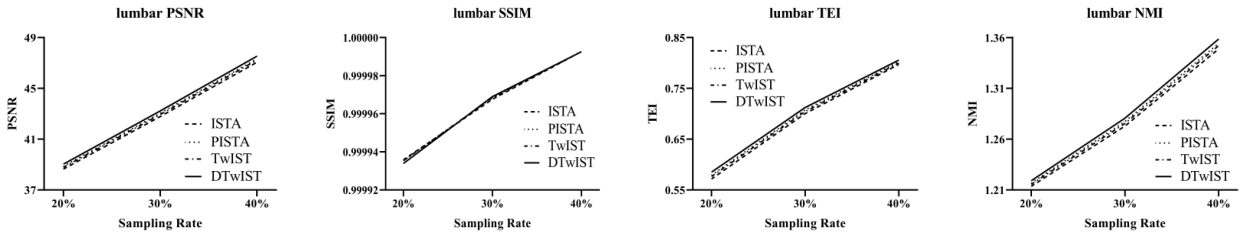

Figure 7. Performance comparison of the different algorithms for lumbar spine MR images under different sampling rates.

In order to further verify the performance of the proposed algorithm, we selected a total of 60 MR images from different slices of the brain, ankle and knee joints for further experiments.

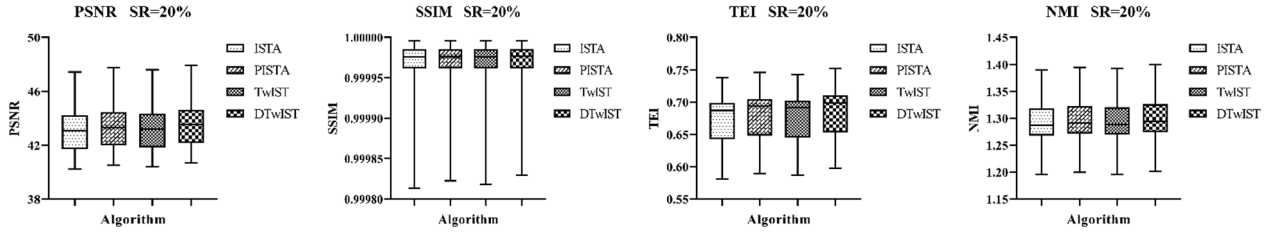

Figure 8. Performance comparison of the different algorithms for 60 MR images at 20% sampling rate.

Figures 8–10 show the box plots of the reconstruction performance of 60 MR images. The sampling rate is 20, 30, 40% respectively. The results show that the proposed algorithm has better reconstruction performance for MR images of other body parts.

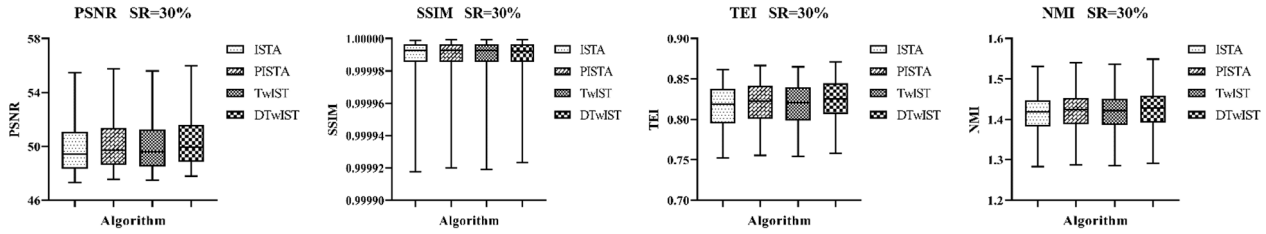

Figure 9. Performance comparison of the different algorithms for 60 MR images at 30% sampling rate.

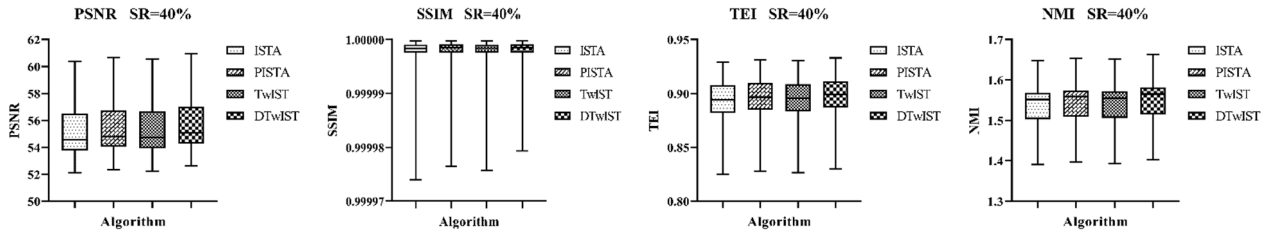

Figure 10. Performance comparison of the different algorithms for 60 MR images at 40% sampling rate.

5. Discussion and conclusions

The proposed algorithm (DTwIST) overcomes the disadvantage that the TwIST algorithm is difficult to balance speed and efficiency. By dynamically adjusting the shrinkage factor, it can greatly accelerate the iterative convergence while ensuring the convergence accuracy.

By compared with ISTA, PISTA, and TwIST in terms of PSNR, SSIM, TEI, NMI and number of iterations, a conclusion can be drawn than the proposed methods can retain more global information and local information of reconstructed images, especially with excellent convergence speed. At the same time, it provides a reference for the improvement of similar algorithms.

Acknowledgments

This work was supported in part by the Jiangsu Provincial Key Research and Development Program under Grant BE2020714, the Postgraduate Research and Practice Innovation Program of Jiangsu Province under Grant KYCX21_1556. Ethical Approval: The Research Ethics Committee of the Nanjing Medical University granted approval for this study and the collection and use of the data analyzed in this study. Approval number: NMUE2021301.

Conflict of interest

The authors declare there is no conflict of interest.

References

1. D. Donoho, Compressed sensing, *IEEE Trans. Inf. Theory*, **52** (2006), 1289–1306. https:// doi.org/10.1109/TIT.2006.871582
2. M. Lustig, D. Donoho, J. M. Pauly, Sparse MRI: The application of compressed sensing for rapid MR imaging, *Magn. Reson. Med.*, **58** (2007), 1182–1195. https://doi.org/10.1002/mrm.21391
3. I. Daubechies, M. Defrise, C. D. Mol, An iterative thresholding algorithm for linear inverse problems with a sparsity constraint, *Commun. Pure Appl. Math.*, **57** (2004), 1413–1457. https://doi.org/10.1002/cpa.20042
4. T. Goldstein, S. Osher, The Split Bregman method for L1-egularized problems, *SIAM J. Imaging Sci.*, **2** (2009), 1–21. https:// doi.org/10.1137/080725891
5. W. W. Hager, H. Zhang, A survey of nonlinear conjugate gradient methods, *Pac. J. Optim.*, **2** (2006), 35–58. https://doi.org/ 10.1006/jsco.1995.1040
6. H. Nien, J. A. Fessler, A convergence proof of the split Bregman method for regularized least-squares problems, *Mathematics*, **2014** (2014). https://doi.org/10.48550/arXiv.1402.4371
7. J. D. Benamou, G. Carlier, M. Cuturi, L. Nenna, G. Peyré, Iterative Bregman projections for regularized transportation problems, *SIAM J. Sci. Comput.*, **37** (2015). https:// doi.org/10.1137/141000439
8. E. G. Birgin, J. M. Martínez, A spectral conjugate gradient method for unconstrained optimization, *Appl. Math. Optim.*, **43** (2001), 117–128. https:// doi.org/10.1007/s00245-001-0003-0
9. M. M. Dehnavi, D. M. Fernandez, D. Giannacopoulos, Enhancing the performance of conjugate gradient solvers on graphic processing units, *IEEE Trans. Magn.*, **47** (2011), 1162–1165. https:// doi.org/10.1109/TMAG.2010.2081662
10. S. Wang, Z. Su, L. Ying, X. Peng, S. Zhu, F. Liang, et al., Accelerating magnetic resonance imaging via deep learning, in *2016 IEEE 13th International Symposium on Biomedical Imaging (ISBI)*, (2016), 514–517. https:// doi.org/10.1109/ISBI.2016.7493320
11. D. Liang, J. Cheng, Z. Ke, L. Ying, Deep magnetic resonance image reconstruction: Inverse problems meet neural networks, *IEEE Signal Process. Mag.*, **37** (2020), 141–151. https:// doi.org/10.1109/MSP.2019.2950557
12. J. M. Bioucas-Dias, M. A. T. Figueiredo, A new twIst: Two-step iterative shrinkage/thresholding algorithms for image restoration, *IEEE Trans. Image Process.*, **16** (2007), 2992–3004. https:// doi.org/10.1109/tip.2007.909319
13. A. Beck, M. Teboulle, A fast Iterative Shrinkage-Thresholding Algorithm with application to wavelet-based image deblurring, in *2009 IEEE International Conference on Acoustics, Speech and Signal Processing*, (2009), 693–696. https:// doi.org/10.1109/ICASSP.2009.4959678
14. Y. Zhang, Z. Dong, P. Phillips, S. Wang, G. Ji, J. Yang, Exponential Wavelet Iterative Shrinkage Thresholding Algorithm for compressed sensing magnetic resonance imaging, *Inf. Sci.*, **322** (2015), 115–132. https:// doi.org/10.1016/j.ins.2015.06.017

15. X. Li, J. Wang, S. Tan, Hessian Schatten-norm regularization for CBCT image reconstruction using fast iterative shrinkage-thresholding algorithm, in *Medical Imaging 2015: Physics of Medical Imaging*, 2015. https:// doi.org/10.1117/12.2082424
16. G. Wu, S. Luo, Adaptive fixed-point iterative shrinkage/thresholding algorithm for MR imaging reconstruction using compressed sensing, *Magn. Reson. Imaging*, **32** (2014), 372–378. https:// doi.org/10.1016/j.mri.2013.12.009
17. K. Shang, Y. Li, Z. Huang, Iterative p-shrinkage thresholding algorithm for low Tucker rank tensor recovery, *Inf. Sci.*, **482** (2019), 374–391. https:// doi.org/10.1016/j.ins.2019.01.031
18. L. Zhang, H. Wang, Y. Xu, A shrinkage-thresholding method for the inverse problem of Electrical Resistance Tomography, in *2012 IEEE International Instrumentation and Measurement Technology Conference Proceedings*, (2012), 2425–2429. https:// doi.org/10.1109/I2MTC.2012.6229564
19. A. Beck, M. Teboulle, A fast iterative shrinkage-thresholding algorithm for linear inverse problems, *SIAM J. Imaging Sci.*, **2** (2009), 183–202. https:// doi.org/10.1137/080716542
20. A. Chambolle, C. Dossal, On the Convergence of the Iterates of the "Fast Iterative Shrinkage/Thresholding Algorithm", *J. Optim. Theory Appl.*, **166** (2015), 1–15. https:// doi.org/10.1007/s10957-015-0746-4
21. İ. Bayram, On the convergence of the iterative shrinkage/thresholding algorithm with a weakly convex penalty, *IEEE Trans. Signal Process.*, **64** (2016), 1597–1608. https:// doi.org/10.1109/TSP.2015.2502551
22. W. Hao, J. Li, X. Qu, Z. Dong, Fast iterative contourlet thresholding for compressed sensing MRI, *Electron. Lett.*, **49** (2013), 1206. https:// doi.org/10.1049/el.2013.1483
23. S. Dirksen, G. Lecue, H. Rauhut, On the gap between restricted isometry properties and sparse recovery conditions, *IEEE Trans. Inf. Theory*, **64** (2018), 5478–5487. https://doi.org/ 10.1109/TIT.2016.2570244
24. Y. Yang, C. M. Kramer, P. W. Shaw, C. H. Meyer, M. Salerno, First-pass myocardial perfusion imaging with whole-heart coverage using L1-SPIRiT accelerated variable density spiral trajectories, *Magn. Reson. Med.*, **76** (2016), 1375–1387. https:// doi.org/10.1002/mrm.26014
25. V. P. Gopi, P. Palanisamy, K. A. Wahid, P. Babyn, D. Cooper, Multiple regularization based MRI reconstruction, *Signal Process.*, **103** (2014), 103–113. https:// doi.org/10.1016/j.sigpro.2013.11.001
26. C. S. Xydeas, V. S. Petrovic, Objective image fusion performance measure, *Electron. Lett.*, **36** (2000), 308–309. https:// doi.org/10.1117/12.381668

AIMS Press